BULLETIN OF THE POLISH ACADEMY OF SCIENCES
TECHNICAL SCIENCES, Vol. 70(1), 2022, Article number: e137509
DOI: 10.24425/bpasts.2021.137509

Bandwidthand power enhancement in the MEMS-based piezoelectric energy harvester using magnetic tip mass

Ashutosh ANAND[1,2*], **Srikanta PAL**[2], and **Sudip KUNDU**[3]

[1] Department of Electronics and Communication Engineering, Presidency University Bangalore, India
[2] Department of Electronics and Communication Engineering, Birla Institute of Technology, Mesra Ranchi, India
[3] Department of Electronics and Communication Engineering and Center for Nanomaterials, National Institute of Technology Rourkela, India

Abstract. In this paper, the performance and frequency bandwidth of the piezoelectric energy harvester (PZEH) is improved by introducing two permanent magnets attached to the proof mass of a dual beam structure. Both magnets are in the vicinity of each other and attached in such a way to proof mass of a dual beam so that they create a magnetic field around each other. The generated magnetic field develops a repulsive force between the magnets, which improves electrical output and enhances the bandwidth of the harvester. The simple rectangular cantilever structure with and without magnetic tip mass has a frequency bandwidth of 4 Hz and 4.5 Hz, respectively. The proposed structure generates a peak voltage of 20 V at a frequency of 114.51 Hz at an excitation acceleration of 1 g (g= 9.8 m/s^2). The peak output power of a proposed structure is 25.5 μW. The operational frequency range of a proposed dual beam cantilever with a magnetic tip mass of 30 mT is from 102.51 Hz to 120.51 Hz, i.e., 18 Hz. The operational frequency range of a dual beam cantilever without magnetic tip mass is from 104.18 Hz to 118.18 Hz, i.e., 14 Hz. There is an improvement of 22.22% in the frequency bandwidth of the proposed dual beam cantilever with a magnetic tip mass of 30 mT than the dual beam without magnetic tip mass.

Key words: vibration; piezoelectric energy harvester; magnetic tip mass; bandwidth; stress.

1. INTRODUCTION

The advancement in the field of VLSI and ever-increasing interest in the Internet of Things (IoT) leads to rapid advancement in the development of miniaturized, low power electronic devices. There are several barriers in the global implementation of IoT, such as the dependency on the conventional battery for the power supply. These batteries have a limited lifespan. Thus, energy harvesting from the ambient energy source became an active research area. The energy harvesting from the vibration of the ambient is the most promising way to power these miniaturized, low-power electronic devices like wireless sensors nodes, biomedical devices, military equipment, etc. The vibration energy harvester (EH) converts vibration energy into useable electric energy. Vibration energy can be converted into electrical energy using electrostatic [1, 2], electromagnetic [3, 4] and piezoelectric (PZ) mechanisms [5–13]. The piezoelectric transducer is the most favoured, as it has high energy density, easy integration in CMOS technology, high durability, and it does not need any external voltage source [10]. There are many EH designs such as cantilever [5, 6], clamped-clamped beams [13], diaphragms [13], cymbal type structure [13], shell and stack type structures [13]. The cantilever structure is the most used as it has higher average strain energy. The rectangular type of cantilever structure is most easy to fabricate and implement. Apart from energy harvesting, piezoelectric materials have been used in several different applications such as buckling [14], stability [14, 15], vibration or loading capacity control [16], tactile sensing [17], etc.

The piezoelectric energy harvester (PZEH) can generate maximum output voltage and power at the resonant frequency. Even the slight change in an ambient frequency can drastically reduce the efficiency of a PZEH. Vast research is done to eliminate this limitation. One such method is the use of nonlinearity in the EH design [18, 19].

One of the methods to introduce nonlinearity is the use of magnetic tip mass as a proof mass in the magnetic environment [19]. The magnet's relative alignment, position, and arrangement can introduce nonlinearity in the system. There are several configurations to improve the efficiency and operating bandwidth of PZEH. The permanent magnet has been used in the EH system to achieve monostable [20,21], bi-stable [22–24] or tri-stable state [25–28] and hence able to increase the operating frequency range. Challa *et al.* [19] designed EH of size 34 mm and tuned the resonant frequency with the magnetic force by changing the relative position of the magnets. Zhou *et al.* [29] try to achieve a penta-stable state by adjusting the position and orientation of the permanent magnet and, hence improving the efficiency. Tan *et al.* [30] try to devise a method to calculate the magnetic force in the piezoelectric energy harvester's vibration and energy harvesting efficiency. Zhu *et al.* [31] designed a (13×5) mm^2 cantilever beam for the

*e-mail: ashunitjsr@gmail.com

Manuscript submitted 2021-03-09, revised 2021-05-10, initially accepted for publication 2021-05-15, published in February 2022.

electromagnetic micro-generator. The resonant frequency of the cantilever has been tuned with the help of the attractive force of the axially aligned permanent magnet. Wei-jiun *et al*. [32] designed a 98 mm dual cantilever to enhance the bandwidth of the EH with a permanent magnet on a dual cantilever. D. Guo *et al*. [33] also designed 12 cm long array of cantilevers to enhance the frequency bandwidth with the magnetic tip mass and increase the performance of EH.

This paper tries to use the concept of multi-beam structure and magnetic field intensity in the EH system to achieve bandwidth improvement. This paper introduces dual magnets in a dual cantilever system. One magnet is attached to the proof-mass of the inner beam, and the other magnet is attached to the outer beam. Both magnets are attached in the vicinity of each other to create the magnetic field intensity and interact with each other. This orientation helps in the improvement of the frequency bandwidth of the EH.

2. ELECTRICAL ANALYSIS OF PIEZOELECTRIC CANTILEVER

A simplified cantilever plate structure consisting of the piezoelectric plate on the top of a substrate layer is considered to develop the analytical model, as shown in Fig. 1. The thickness of the substrate layer is t_S, and that of the piezoelectric layer is t_P. The effect of the electrode is neglected in the analytical model due to its small thickness.

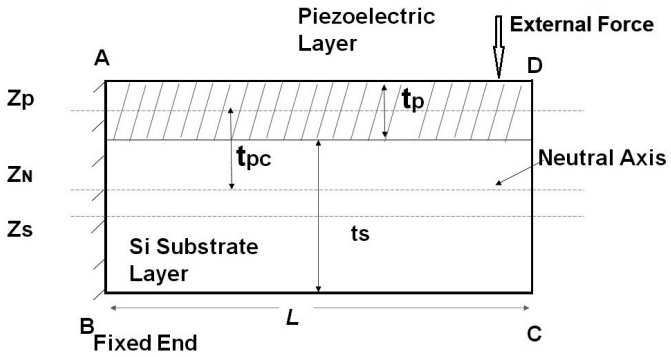

Fig. 1. A simplified version of the basic cantilever

In a PZ material, the external force on the PZ layer generates an electric field and vice versa. When the PZ cantilever operates in 31 modes, stress generates in the lateral direction (X direction or 3 direction) and an electric field in the transverse direction (Z direction or 1 direction). So, equations (1a) and (1b) show the PZ property and inverse PZ property [5, 6].

$$S_1 = s_{11}^E T_1 + d_{31} E_3\,, \tag{1a}$$

$$D_3 = d_{31} T_1 + \varepsilon_{33}^T E_3\,, \tag{1b}$$

where S_1 is mechanical strain generated in the PZ material and D_3 is the electric displacement in the PZ materials under given mechanical stress T_1 and electric field E_3. s_{11}^E is strain under zero or constant electric field, ε_{33}^T is the permittivity of the material under zero or constant stress, and d_{31} is the PZ coefficient.

The substrate layer is the normal linear elastic material, so the stress applied (T_s) in the substrate layer is directly proportional to the resultant strain (S_s) as

$$T_s = Y_s S_s\,. \tag{2}$$

But, in the case of the PZ material, applied stress (T_p) not only induces strain (S_p) but also generates an electric field (E). When the rectangular cantilever structure vibrates vertically, stress acts in the x, y and xy plane. So, the applied stress, strain and electric field in the PZ layer are related as in equations (3) (a, b, c) [5, 6].

$$T_{pxx} = \frac{Y_p}{1-\upsilon^2} S_{pxx} + \frac{\upsilon Y_p}{1-\upsilon^2} S_{pyy} - d_{31} Y_P E\,, \tag{3a}$$

$$T_{pyy} = \frac{Y_p}{1-\upsilon^2} S_{pyy} + \frac{\upsilon Y_p}{1-\upsilon^2} S_{pxx} - d_{32} Y_P E\,, \tag{3b}$$

$$T_{pxy} = G S_{pxx} - (d_{31} + d_{32}) Y_p E\,, \tag{3c}$$

where υ is the poison ratio, G is the shear modulus, and Y_p is the Young's Modulus of the PZ layer.

When the cantilever plate is subject to external stress, it deflects from the mean position or neutral axis. This induces the bending strain in the layer away from the neutral axis. Equations 4a, 4b, 4c show the cantilever plates' bending strain [5, 6].

$$S_{pxx} = -(Z_N - Z)\frac{\partial^2 w(x,y,t)}{\partial x^2}\,, \tag{4a}$$

$$S_{pyy} = -(Z_N - Z)\frac{\partial^2 w(x,y,t)}{\partial y^2}\,, \tag{4b}$$

$$S_{pxy} = -2(Z_N - Z)\frac{\partial^2 w(x,y,t)}{\partial x \partial y}\,, \tag{4c}$$

where Z_N is the neutral plane and $(Z_N - Z) = t_{PC}$ is the distance from the neutral surface to the material point of interest, $w(x,y,t)$ is the transverse displacement of the cantilever structure.

Putting the value of strain from equation (4a, 4b, 4c) into equation (3a, 3b, 3c) [5, 6], we have.

$$T_{pxx} = \frac{Y_p}{1-\upsilon^2}\left(-t_{PC}\frac{\partial^2 w(x,y,t)}{\partial x^2}\right) + \frac{\upsilon Y_p}{1-\upsilon^2}\left(-t_{PC}\frac{\partial^2 w(x,y,t)}{\partial y^2}\right) - d_{31} Y_p E\,, \tag{5a}$$

$$T_{pxx} = \frac{Y_p}{1-\upsilon^2}\left(-t_{PC}\frac{\partial^2 w(x,y,t)}{\partial y^2}\right) + \frac{\upsilon Y_p}{1-\upsilon^2}\left(-t_{PC}\frac{\partial^2 w(x,y,t)}{\partial x^2}\right) - d_{32} Y_p E\,, \tag{5b}$$

$$T_{pxy} = G\left(-2t_{PC}\frac{\partial^2 w(x,y,t)}{\partial x \partial y}\right) - (d_{31} + d_{32}) Y_p E\,. \tag{5c}$$

The value of stress from equations (5a, 5b, 5c) is substituted in equation (1b) to obtain the electric displacement in x, y and

xy plane. Equation (6) shows the electric displacement due to stress in the x plane [5, 6].

$$D_{zx} = d_{31}\left[\frac{Y_p}{1-\upsilon^2}\left(-t_{PC}\frac{\partial^2 w(x,y,t)}{\partial x^2}\right) + \frac{\upsilon Y_p}{1-\upsilon^2}\left(-t_{PC}\frac{\partial^2 w(x,y,t)}{\partial y^2}\right) - d_{31}Y_p E\right] + \varepsilon_{33}^T E. \quad (6)$$

The charge generated in the piezoelectric plate is given by equation (7) [5, 6],

$$\begin{aligned} Q_{\text{Total}}(t) &= d_{31}\int_0^L\int_0^b\left[\frac{Y_p t_{PC}}{1-\upsilon^2}\left\{\left(-\frac{\partial^2 w(x,y,t)}{\partial x^2}\right) + \upsilon\left(-\frac{\partial^2 w(x,y,t)}{\partial y^2}\right)\right\} + \left(\varepsilon_{33}^T - d_{31}Y_p\right)E\right]\mathrm{d}x\mathrm{d}y \\ &= d_{31}\int_0^L\int_0^b\left[\frac{Y_p t_{PC}}{1-\upsilon^2}\left\{\left(-\frac{\partial^2 w(x,y,t)}{\partial x^2}\right) + \upsilon\left(-\frac{\partial^2 w(x,y,t)}{\partial y^2}\right)\right\} + \varepsilon_{31}^s\frac{V(t)}{t_p}\right]\mathrm{d}x\mathrm{d}y, \end{aligned} \quad (7)$$

where $(\varepsilon_{33}^T - d_{31}Y_p) = \varepsilon_{31}^s$, $E = \dfrac{V(t)}{t_p}$, t_p is a thickness of PZ layer, $V(t)$ is the voltage generated in PZ layer.

Thus, total current generated in this plate is $I(t) = \dfrac{\partial Q_{\text{Total}}(t)}{\partial t}$. If R is the internal resistance of PZ plate, so according to the ohm's law the voltage generated in PZ plate is given by $V_1(t) = I(t) \times R$, [5, 6].

$$V_1(t) = -R\int_0^L\int_0^b d_{31}\left[\frac{Y_p t_{PC}}{1-\upsilon^2}\left\{\left(\frac{\partial^2 w(x,y,t)}{\partial x^2 \partial t}\right) + \upsilon\left(\frac{\partial^2 w(x,y,t)}{\partial y^2 \partial t}\right)\right\} - \frac{\varepsilon_{31}^s}{t_p}\frac{\partial V(t)}{\partial t}\right]\mathrm{d}x\mathrm{d}y. \quad (8)$$

Similarly, the voltage generated in a PZ layer due to the stress in y and xy plane can be evaluated as [5, 6].

$$V_2(t) = -R\int_0^L\int_0^b d_{32}\left[\frac{Y_p t_{PC}}{1-\upsilon^2}\left\{\left(\frac{\partial^2 w(x,y,t)}{\partial x^2 \partial t}\right) + \upsilon\left(\frac{\partial^2 w(x,y,t)}{\partial y^2 \partial t}\right)\right\} - \frac{\varepsilon_{32}^s}{t_p}\frac{\partial V(t)}{\partial t}\right]\mathrm{d}x\mathrm{d}y, \quad (9)$$

$$V_3(t) = -R\int_0^L\int_0^b (d_{31}+d_{32})\left[G t_{PC}\left(\frac{\partial^2 w(x,y,t)}{\partial x \partial y \partial t}\right) - \frac{(\varepsilon_{31}^s + \varepsilon_{32}^s)}{t_p}\frac{\partial V(t)}{\partial t}\right]\mathrm{d}x\mathrm{d}y. \quad (10)$$

The total voltage is generated across the PZ layer of the cantilever as in equation (11) [5, 6].

$$V_4(t) = V_1(t) + V_2(t) + V_3(t). \quad (11)$$

So, from the above discussion (equations (7), (8), (9), (10) and (11)), it can be concluded that the electric voltage develops across the PZ layer depending on the stress distribution on the cantilever beam. So, when all the other design parameters are the same, the cantilever structure with a higher stress distribution gives a higher voltage than the others. The introduction of the magnetic field in the PZ cantilever system with the help of the magnetic tip mass will increase the stress distribution and improve the performance of the PZEH.

3. MECHANICAL MODELLING OF PZEH WITH MAGNET TIP MASS

The PZEH with a permanent magnet attached to the proof mass is axially aligned with the fixed magnet. Kirchhoff plate theory with additional magnetic force is used to model the system [5, 6]. The magnetic force in the PZEH produces the nonlinear restoring force.

The mechanical deviation of the cantilever plate in perpendicular direction can be expressed as equation (12a or 12b) [5, 6, 34].

$$D_r\left(\frac{\partial^4 w(x,y,t)}{\partial x^4} + 2\frac{\partial^4 w(x,y,t)}{\partial x^2 \partial y^2} + \frac{\partial^4 w(x,y,t)}{\partial y^4}\right) + \rho t_p\frac{\partial^2 w(x,y,t)}{\partial t^2} = f(x,y,t)_m, \quad (12a)$$

or,

$$D_r\nabla^4 w(x,y,t) + \rho t_p\frac{\partial^2 w(x,y,t)}{\partial t^2} = f(x,y,t)_m, \quad (12b)$$

where ∇^4 is the biharmonic operator and is given in equation (13), $w(x,y,t)$ is the vertical displacement of the plate, ρ is the density, D_r is the flexural rigidity which is given in equation (14). $f(x,y,t)_m$ is the magnetic force between the magnets in the system at any deflection $w(x,y,t)$, is given by equation (15) [5, 6, 34].

$$\nabla^4 = \nabla^2\nabla^2 = \frac{\partial^4}{\partial x^4} + 2\frac{\partial^4}{\partial x^2 \partial y^2} + \frac{\partial^4}{\partial y^4}, \quad (13)$$

$$D_r = \frac{Y t^3}{12(1-\upsilon^2)}, \quad (14)$$

$$f(x,y,t)_m = -\frac{3\mu_0 m_1 m_2}{2\pi(D + w(x,y,t))^4}, \quad (15)$$

where m_1 and m_2 are the magnetic dipole which is given as $m_i = \dfrac{2BV_v}{\mu_0}$, $i = 1, 2$. μ_0 ($= 4\pi \times 10^{-7}$ H/m) is the permeability of the air and two magnets are D distance apart and V_v is the volume of the magnets.

There will be the repulsive force when both magnets are of same magnetic polarization and attractive in nature when the magnets are of opposite magnetic polarization.

When there is no magnetic force acting in the cantilever system, the $f(x,y,t)_m$ is taken as zero in equation (12). This is the

case of free vibration of a cantilever plate [5, 6, 34] as

$$D_r \nabla^4 w(x,y,t) + \rho t_p \frac{\partial^2 w(x,y,t)}{\partial t^2} = 0. \tag{16}$$

The length and width of the rectangular plate is L and b, so the boundary limit along the length varies from $x = 0$ to L and along the width is $y = 0$ to b. When the external magnetic force ($f(x,y,t)$) will be considered then the solution of displacement of the rectangular cantilever i.e., equation (12) will be considered as [5, 6, 34].

$$D_r \nabla^4 w(x,y,t) + \rho t_p \frac{\partial^2 w(x,y,t)}{\partial t^2} = -\frac{3\mu_0 m_1 m_2}{2\pi(D+w(x,y,t))^4}. \tag{17}$$

According to the vertical displacement of the plate we have,

$$w(x,y,t) = \sum_{m=1}^{\infty}\sum_{n=1}^{\infty} w_{mn}(x,y) T_{mn}(t), \tag{18}$$

where,

$$w_{mn}(x,y) = B_{1mn} \sin\frac{m\pi x}{L} \sin\frac{n\pi y}{b}; \quad m,n = 1,2\ldots \tag{19}$$

The normalization condition that the normal nodes will satisfy is given as [5, 6, 34],

$$\int_0^L \int_0^b \rho t_p w_{mn}^2 \,\mathrm{d}x\,\mathrm{d}y = 1, \tag{20}$$

which yields $B_{1mn} = \dfrac{2}{\sqrt{\rho t_p L b}}$. By using normalization condition in equation (20) and substituting it into equation (12), we obtained the equation of the governing the generalized coordinates $T_{mn}(t)$ as [5, 6, 34],

$$\frac{\partial^2 T_{mn}(t)}{\partial t^2} + \omega_{mn}^2 T_{mn}(t) = N_{mn}(t); \quad m,n = 1,2\ldots, \tag{21}$$

where $N_{mn}(t)$ is the generalized force and the natural frequency ω_{mn} is given by [5, 6, 34],

$$N_{mn}(t) = \int_0^L \int_0^b w_{mn}(x,y) f(x,y,t)_m \,\mathrm{d}x\,\mathrm{d}y, \tag{22}$$

$$\omega_{mn} = \pi^2 \left(\frac{D_r}{\rho t_p}\right)^{1/2} \left[\left(\frac{m}{L}\right)^2 + \left(\frac{n}{b}\right)^2\right]; \quad m,n = 1,2\ldots \tag{23}$$

The solution of equation (21) can be expressed as (24) [5, 6, 34],

$$T_{mn}(t) = T_{mn}(0)\cos\omega_{mn}t + \frac{1}{\omega_{mn}}\frac{\partial T_{mn}(t)}{\partial t}\sin\omega_{mn}t + \frac{1}{\omega_{mn}}\int_0^t N_{mn}(\tau)\sin\omega_{mn}(t-\tau)\,\mathrm{d}\tau. \tag{24}$$

The final solution of the rectangular plate vibration under external force is given by equation (25) [5, 6, 34].

$$\begin{aligned} w(x,y,t) = {} & \sum_{m=1}^{\infty}\sum_{n=1}^{\infty} T_{mn}(0)\sin\frac{m\pi x}{L}\sin\frac{n\pi y}{b}\cos[\omega_{mn}t] \\ & + \sum_{m=1}^{\infty}\sum_{n=1}^{\infty}\frac{\partial T_{mn}(0)}{\partial t}\frac{1}{\omega_{mn}}\sin\frac{m\pi x}{L}\sin\frac{n\pi y}{b}\sin[\omega_{mn}t] \\ & + \sum_{m=1}^{\infty}\sum_{n=1}^{\infty}\frac{1}{\omega_{mn}}\sin\frac{m\pi x}{L}\sin\frac{n\pi y}{b} \\ & \int_0^t T_{mn}(\tau)\sin[\omega_{mn}(t-\tau)]\,\mathrm{d}\tau. \end{aligned} \tag{25}$$

Thus, it can be observed that the deflection of the end mass of the vibrating dual beam cantilever structure depends on the magnetic force (from equations (22), (24) and (25)). Hence the magnetic effect influences the vibration of the cantilever structure.

4. DESIGN OF THE CANTILEVER STRUCTURE

4.1. Design of the single beam structure

The rectangular cantilever structure is designed with silicon as the substrate and zinc oxide as the PZ layer. The proof mass is at the tip of the free end of the cantilever consisting of Si and a permanent magnet (PM1), which helps reduce the resonant frequency [5], as shown in Fig. 2. Another fixed magnet (PM2) is placed axially in the vicinity of the first magnet to create repulsive magnetic force [4]. The permanent magnet can act as a spring which produces nonlinearity in the system. Table 1 and Table 2 comply with all the dimensions and properties of

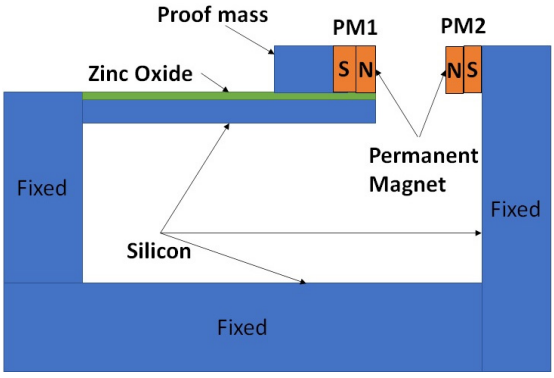

Fig. 2. Single rectangular cantilever beam with magnetic tip mass

Table 1
The geometry of different materials used in the single beam cantilever

	Si	ZnO	PROOF MASS		PM2
			Si	PM1	
Length (μm)	5000	5000	800	200	200
Width (μm)	1000	1000	1000	1000	1000
Thickness (μm)	12	2	850	850	850

the materials used to design the cantilever plate. The magnetic field intensity of the magnets used in the design of the simple rectangular structure is 5 mT. Both the magnets are 500 μm apart. The COMSOL Multiphysics 5.3a is used to design the cantilever structure. The structure has meshed as the normal meshing techniques. Solid mechanics and electrostatics physics are used to obtain the designed cantilever structure's mechanical and electrical characterization. The resonant frequency of the simple single rectangular cantilever structure is 95.5 Hz, and that of the simple single rectangular cantilever with magnetic tip mass structure is 95 Hz, which agrees with the above discussion.

Table 2
Property of the materials used in the cantilever beam [5, 8, 9]

Property	MATERIALS		
	Si	ZnO	Permanent Magnet
Young's Modulus (GPa)	170	210	0.1
Poisson ratio	0.29	0.33	0.29
Density (kg/m^3)	2329	5680	7500

Before moving to the design of the dual beam structure, we first try to verify the effect of the magnetic field intensity on the stress distribution. For that, we have taken the designed simple rectangular cantilever of dimensions as shown in Fig. 2 and Table 1. The stationary study is employed on the designed cantilever structure to verify the effect of magnetic field intensity on the stress distribution. The first stationary study is employed with a fixed load of 1g ($= 9.8$ m/s^2); only then, the magnetic field intensity is gradually introduced in the system to study its effect. Figure 3 shows the stress distribution along the arc length of the cantilever structure. It can be observed from Fig. 3 that the stress distribution increases with the increase in the magnetic field intensity, which agrees with the above discussed mathematical analysis.

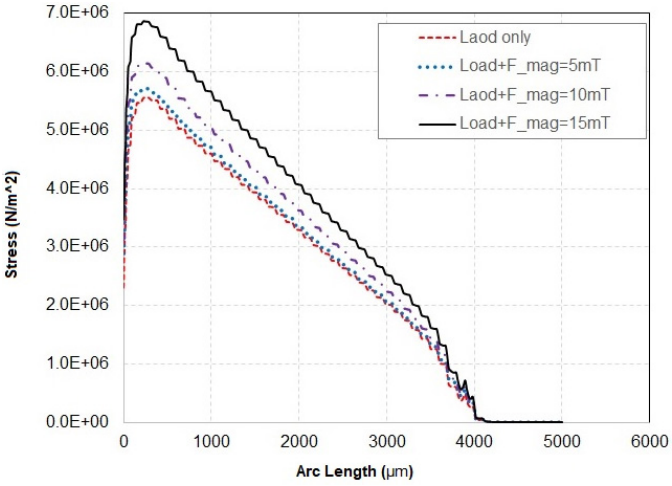

Fig. 3. Variation of stress along arc length with magnetic field intensity

4.2. Design of the dual beam structure

The rectangular-shaped dual beam EH is designed to improve the bandwidth of the EH. The cantilever has Si as substrate and ZnO as the PZ material. The proof mass is attached at the free end of the dual beam structure to reduce the resonant frequency. The permanent magnet is attached to each of the proof masses, such that they create the repulsive magnetic force around each other. Figure 4 shows the arrangement of proof mass with a permanent magnet. The magnetic field intensity of the magnet used in the dual beam structure is the same as that of the single beam cantilever structure. The inner beam ($L2$), outer beam, and ($L1$) are 4200 μm and 5000 μm, respectively. The width of the arm of the outer beam ($W3$) connected to the fixed end is 500 μm, and the arm at the free end ($W4$) is 600 μm. The width of the inner beam ($W2$) is 1000 μm. The overall width of the dual beam ($W1$) is 2500 μm. The total thickness of the dual cantilever beam is 14 μm. The Si substrate and ZnO thicknesses are 12 μm and 2 μm, respectively. The ZnO is distributed uniformly throughout the cantilever surface. The dimension of the proof mass connected to the inner beam (IPM) is $1000 \times 1000 \times 850$ μm^3, which consists of Si and a permanent magnet (PM3). The Si and permanent magnet length is 800 μm and 200 μm, while width and thickness remain the same. The proof mass of the outer beam (OPM) also consists of Si and a permanent magnet (PM4). The net dimension of the proof mass of the outer beam is $600 \times 1000 \times 850$ μm^3. The length of the Si layer is 400 μm, and that of the permanent magnet is 200 μm, while width and thickness remain the same. The gap between the inner and outer beam is 250 μm, and the distance between the two magnets is 200 μm. The perforation is introduced at the proper position in the inner and outer beam to reduce the resonant frequency and brings their resonant frequency closer to each other [5]. The length (L_4) and width (W_4) of the perforation in the outer arm are 800 μm and 100 μm, respectively, whereas length (L_3) and width (W_3) of perforation of the inner arm is 1000 μm and 400 μm, respectively. The properties and the complete dimension of the materials used in the dual beam design are listed in Table 2 and Table 3, respectively. The first two eigen frequencies of the dual beam with the magnetic tip mass and without magnetic tip mass are 107.51 and 114.51 Hz.

Table 3
Dimension of the dual beam

	Inner arm		Outer arm		IPM		OPM	
	Si	ZnO	Si	ZnO	Si	PM3	Si	PM4
Length (μm)	$L1 = 4200$		$L1 = 5000$		800	200	400	200
Width (μm)	$W2 = 1000$		$W3 = 500$, $W4 = 600$		1000		1000	
Thickness (μm)	12	2	12	2	850		850	

The electrical output of the PZEH depends on the average stress distribution in the cantilever structure, as shown by equations (1b), (6) and (7). Figure 5 shows the comparison between the stress distribution of different cantilever structures at their

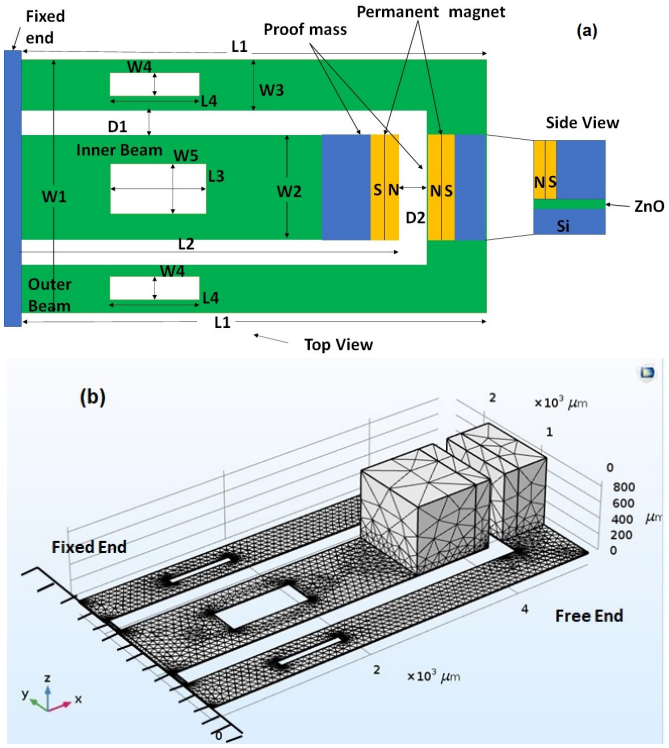

Fig. 4. (a) Top View dual beam structure with perforation (b) 3D view of meshed dual beam structure with perforation

respective resonant frequency. The stress distribution of the dual beam is plotted to varying values of magnetic field intensity, as shown in Fig. 5. The stress distribution is highest in the dual beam cantilever structure with magnetic tip mass at 30 mT magnetic field intensity at its resonant frequency. It can be concluded by Fig. 5 that the stress distribution within the cantilever increases with the increase in the magnetic intensity of the tip mass.

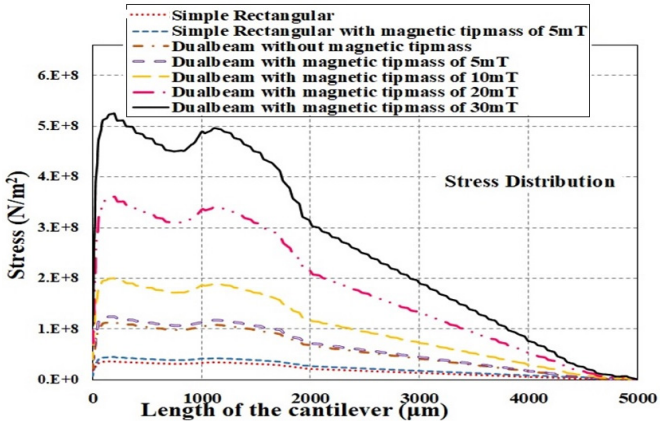

Fig. 5. Stress in different cantilever beams

The stress distribution in the cantilever beam increases when the magnetic intensity of the permanent magnet increases. The maximum stress developed in the cantilever beam should be less than Young's Modulus of the materials used in the cantilever design. The elastic nature in the materials and mechanical strength of the cantilever will be compromised if the stress distribution within the cantilever is higher than Young's Modulus. Figure 5 shows the stress distribution of all the cantilevers, suggesting that all the cantilevers have sufficient mechanical strength.

5. ELECTRICAL OUTPUT ANALYSIS OF THE CANTILEVER STRUCTURES

5.1. Output Voltage analysis of cantilever structures

The PZ-based energy harvester generates the maximum output voltage and power at the resonant frequency, given by equation (23). Therefore, a time-domain analysis is carried out at a respective resonant frequency of all the rectangular cantilever structures with and without magnetic tip mass and for dual cantilever beams with and without magnetic tip mass in COMSOL Multiphysics. The transient analysis gives the time-dependent voltage. A sinusoidal acceleration of 1 g ($g = 9.8\ ms^{-2}$) is applied to all structures at their respective resonant frequency. Figure 6 shows all the cantilever structures' time-varying output voltage at their resonant frequency.

The peak output voltage of a simple rectangular cantilever beam is 18.4 V at its resonant frequency, i.e., 96 Hz. The rectangular cantilever with a 5 mT magnetic tip mass is 21.2 V at its corresponding resonant frequency of 95.5 Hz. It can be observed that with the introduction of the magnetic effect in the cantilever structure, the output voltage increases. The paper's focus is to improve the bandwidth, so the higher magnetic field intensity is only used in the dual beam cantilever structure. Similarly, transient analysis on the dual beam is carried out by applying a sinusoidal acceleration of 1g (g is the acceleration due to gravity) and varying the frequency of the cantilever structure. It is observed that the peak output voltage of the simple dual beam cantilever structure is 12 V at the frequency of 115.18 Hz, and that of the dual beam with a magnetic tip mass of 5 mT is 14 V at the frequency of 115 Hz. The peak output voltage of dual beam with magnetic tip mass of 10 mT, 20 mT, and 30 mT is 16.4 V, 18.5 V, and 20 V at their respective resonant frequency of 114.81 Hz, 114.61 Hz, and 114.31 Hz.

5.2. Output Power analysis of the cantilever structure

The maximum output power is generated by PZEH when the structure's resonant frequency matches the ambient frequency. The other necessary condition is the value of optimum load resistance, which is the same as that of the internal resistance [1, 5–7]. The simple rectangular cantilever's internal resistance will be the same as the rectangular cantilever with a magnetic tip mass since both configurations have the same dimension. Similarly, the internal resistance of all dual beam cantilever structures will be the same irrespective of magnetic field intensity. The electrical equivalent of a single beam piezoelectric cantilever is represented in Fig. 7.

The dual beam's inner beam and outer beam are connected in a parallel configuration. So, the electrical equivalent of the coupled plate structure can also be represented as a parallel combination of two current sources, two capacitors, and two resistors, as shown in Fig. 8.

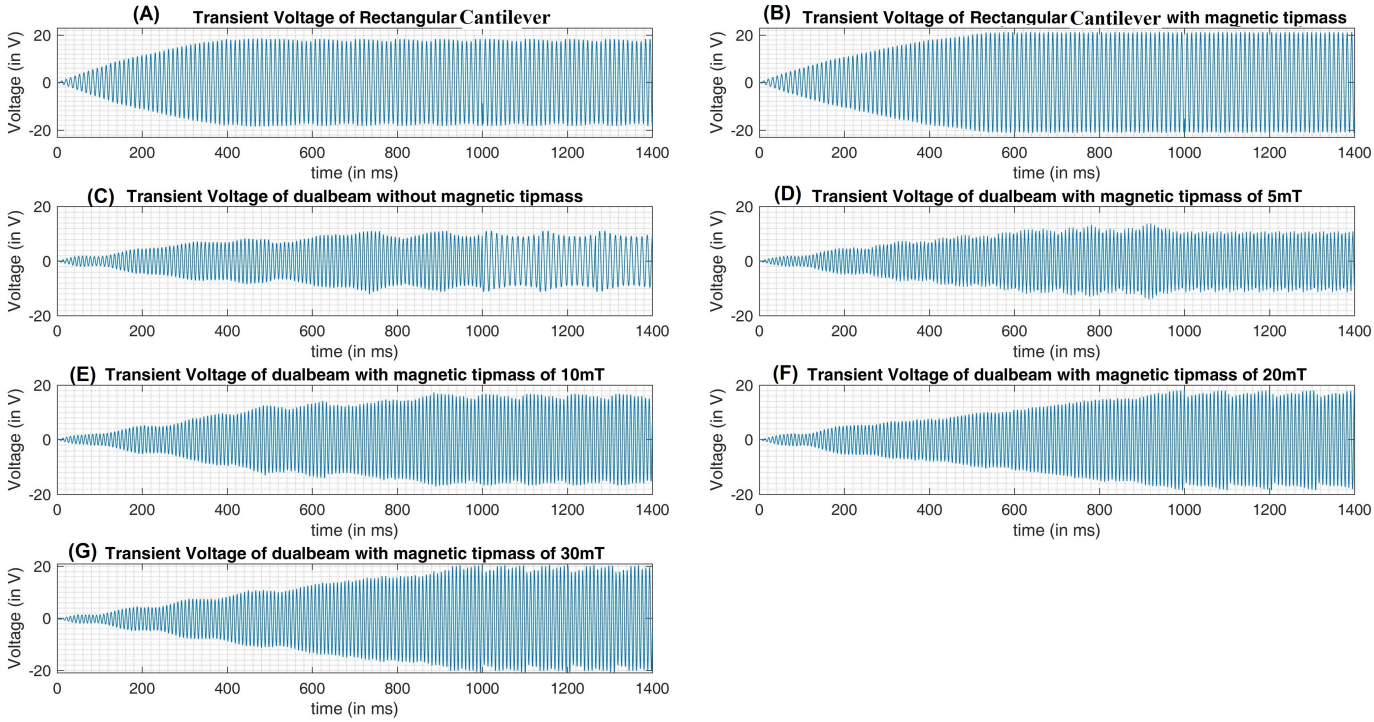

Fig. 6. Transient voltage of (a) simple rectangular, (b) rectangular with magnetic tip mass, (c) dual beam without magnetic tip mass, (d) dual beam with magnetic tip mass of 5 mT, (e) dual beam with magnetic tip mass of 10 mT, (f) dual beam with magnetic tip mass of 20 mT, (g) dual beam with magnetic tip mass of 30 mT

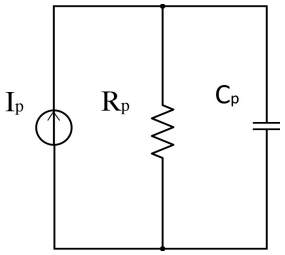

Fig. 7. Electrical equivalent model of a PZ Cantilever Plate

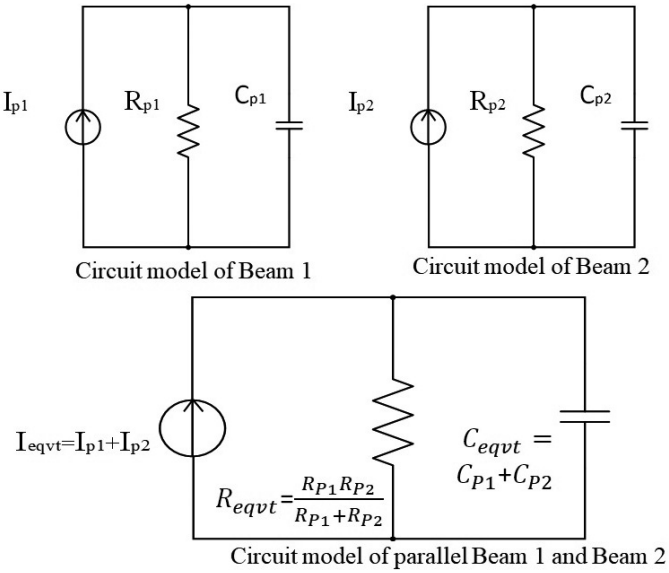

Fig. 8. Electrical equivalent circuit model for coupled dual beam structure

The equivalent capacitor of the equivalent circuit is the sum of the individual capacitors. The reciprocal of equivalent resistance is equal to the sum of the reciprocal of individual resistance. Since there is no direct method to find the internal resistance, it will be calculated indirectly. The PZEH will generate maximum power when the load resistance is equal to the internal resistance of PZEH. This load resistance is called optimum load resistance. The optimum load resistance is calculated by simulating the PZEH at the resonant frequency by varying the load resistance. The graph of the output power of different cantilever structures at varying load resistance is plotted. The position at which the maximum output power is achieved for the given load resistance will give the optimum load. Figure 9 shows the graph between the output power variation with the load resistance. It may be observed from the graph that the optimum load for the simple rectangular and rectangular with magnetic tip mass has an optimum load of 2 MΩ, and the optimum load for the inner arm and outer arm of the dual beam are 1.6 MΩ and 1.3 MΩ. Hence the equivalent internal resistance of the dual beam is 0.72 MΩ.

The maximum power is calculated at this optimum load resistance. The average output power is calculated by calculating the ratio of the average square of the transient voltage obtained at the particular frequency with the optimum resistance of the

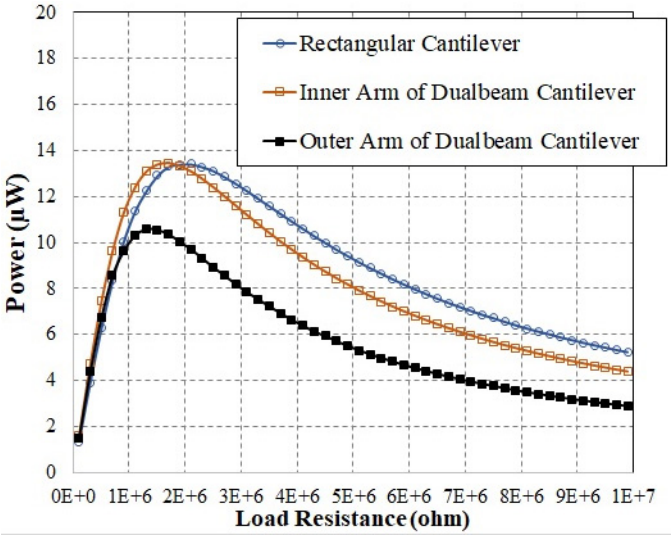

Fig. 9. Variation of Output Power with Load Resistance

cantilever structure. Figure 10 shows the variation of the average output power with the frequency for all the different structures in the same graph.

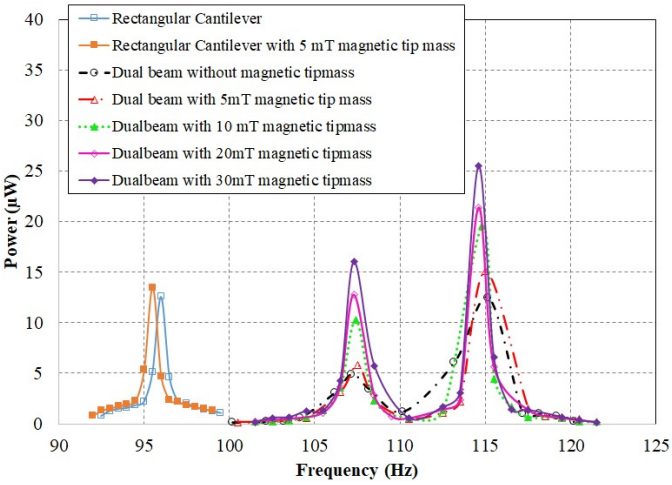

Fig. 10. Variation of output power with frequency for all cantilever structures

The dual beam's output power and output voltage have two peaks at 107.51 Hz and 114.51 Hz. There is a dip in the output voltage and output power at 110.51 Hz. This dip in the voltage and power may be due to the out-of-phase motion of the dual beam. The peak voltage and power at frequencies 107.51 Hz and 114.51 Hz may be due to the in-phase motion of the dual beam.

Since the stress distribution increases with the increase in the magnetic field intensity in the cantilever, as shown in Fig. 5. So, the output power of the cantilever structures increases with the increase in the magnetic field intensity, as shown in Fig. 10. Also, it can be observed from Fig. 5 that there is an increase in stress distribution along the length of the cantilever when the magnetic field intensity increases. So, there may be a possibility that the strength of the cantilever can be compromised when the magnetic intensity of the magnet increases abruptly. So, there should be the optimum magnetic field strength that can be applied while designing the EH system.

The combined output voltage plot of all cantilever structures is plotted together in the same frequency scale. This plot gives the working bandwidth (or frequency range) of all the cantilever structures. The output voltage of all cantilever structures is shown in Fig. 11.

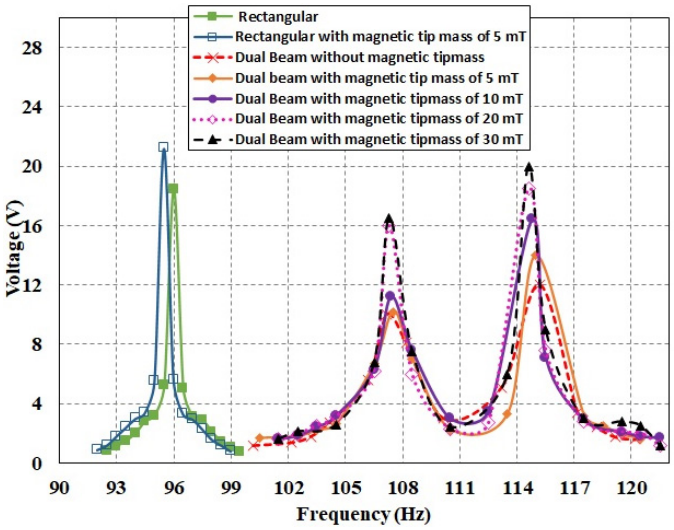

Fig. 11. Variation of output voltage with frequency for all cantilever structures

The bandwidth of operation is assumed as the frequency range at which the output voltage is greater than 2 V as most of the low power devices can efficiently run with a 2 V power supply. The bandwidth of all the structures discussed here is tabulated in Table 4. It can be observed that the single cantilever structures, i.e., simple rectangular and simple rectangular with 5 mT magnetic intensity, have the bandwidth of 4 Hz (94 Hz–98 Hz) and 4.5 Hz (93 Hz–97.5 Hz), respectively. The operating bandwidth of the dual beam structure without magnetic tip mass has a bandwidth of 14 Hz (104.18 Hz–118.18 Hz). The introduction of the magnetic tip mass in the dual beam structure increased the operating frequency range of the cantilever. The bandwidth of the dual beam with a magnetic tip mass of 5 mT, 10 mT, 20 mT, and 30 mT are 14 Hz, 15 Hz, 16 Hz, 17 Hz, and 18 Hz, respectively. It must be noted that in the dual beam structure, each beam must have a different resonant frequency. The resonant frequency of each beam in the dual beam must be close so that the structures can produce voltage over the wide frequency range. So, if the proper cantilever beam is not selected while designing the dual beam then wideband energy harvester will not be achieved. Finally, the proposed work is compared with the available literature in Table 5. It can be observed from the table that the present work has been able to achieve higher or comparable bandwidth and shows an improvement in the performance with EH with a smaller dimension than the reported literature.

Table 4
Bandwidth of all thestructure

Structures	Bandwidth	Peak Voltage (V)	Average power (μW)
Simple Rectangular Cantilever	4 Hz (94–98 Hz)	18.4	12.614
Rectangular cantilever with magnetic tip mass of 5 mT	4.5 Hz (93–97.5 Hz)	21.2	13.52
Dual beam without magnetic tip mass	14 Hz (104.18–118.18 Hz)	12	12.42
Dual beam with magnetic tip mass of 5 mT	15 Hz (103.51–118.51 Hz)	14	15.12
Dual beam with magnetic tip mass of 10 mT	16 Hz (103.51–119.51 Hz)	16.4	19.58
Dual beam with magnetic tip mass of 20 mT	17 Hz (103.51–120.51 Hz)	18.5	21.4
Dual beam with magnetic tip mass of 30 mT	18 Hz (102.51–120.51 Hz)	20	25.5

Table 5
Comparison of the proposed work with the existing literature

Ref (year)	Dimension	Bandwidth	Electrical output
[19] Challa *et al.* (2008)	Beam – $34 \times 20 \times 0.6$ mm^3	10 Hz (22–32 Hz)	Power – 240–280 μW
[31] Zhu *et al.* (2010)	Beam – $13 \times 5 \times 0.12$ mm^3	30.4 Hz (67.6–98 Hz)	Power – 61.6–156.6 μW
[32] W. Su *et al.* (2014)	Length 98 mm, width 20 mm, thickness 0.531 mm	3.8 Hz (10–13.8 Hz)	Power – 1.8 mW
[33] Guo *et al.* (2016)	Beam 1 – $120 \times 20 \times 2$ mm^3 Beam 2 – $120 \times 20 \times 1$ mm^3	14 Hz (28–42 Hz)	Beam 1 Voltage – 24.84 V, Power – 81.97 mW/g^2; Beam 2 Voltage – 18.36 V, Power – 44.78 mW/g^2
This work	$5 \times 2.5 \times 0.014$ mm^3	18 Hz (102.51–120.51 Hz)	Voltage – 20 V, Power – 25.50 μW

6. CONCLUSION

In this paper, the effect of magnetism in the piezoelectric cantilever beam with magnetic tip mass has been discussed. The article shows an improvement not only in terms of the electrical output, which includes the output voltage and output power of the harvester but also it helps in improving the operating frequency range of the harvester. In this paper, a single beam rectangular structure with and without magnetic tip mass is simulated, which enhances the harvester's electrical output. The dual beam structure is simulated with and without the magnetic tip mass in the COMSOL Multiphysics, which also improves the output voltage and power. The dual beam structure also shows an improvement in the frequency bandwidth with the introduction of the magnetic field intensity. The increase in the magnetic field intensity improves the output voltage and power of the dual beam structures. There is a significant improvement in the frequency bandwidth of the dual beam structures compared to the single beam rectangular structures. The operational frequency bandwidth of the dual beam cantilever with a magnetic tip mass of 30 mT is 18 Hz as compared to the simple rectangular cantilever with or without the magnetic tip mass, which has the operational frequency bandwidth of 4.5 Hz and 4 Hz. The operating frequency range of the proposed dual beam cantilever with magnetic tip mass is from 102.51 Hz to 120.51 Hz. The proposed dual beam's output power and output voltage with a magnetic tip mass of 30 mT is 25.5 μW and 20 V, respectively.

This article uses the concept of a multi-beam structure using the magnetic field strength in the EH system to improve the bandwidth. The use of an efficient electrode design can further enhance the efficiency of EH. Another way to change the orientation and position of a permanent magnet to enhance the bandwidth further.

REFERENCES

[1] P. Glynne-Jones, M.J. Tudor, S.P. Beeby, and N.M. White, "An electromagnetic, vibration-powered generator for intelligent sensor systems", *Sens. Actuators, A*, vol. 110, no. 1–3, pp. 344–349, 2004, doi: 10.1016/j.sna.2003.09. 045.

[2] P.D. Mitcheson, P. Miao, B.H. Stark, E.M. Yeatman, A.S. Holmes, and T.C. Green, "MEMS electrostatic micropower generator for low frequency operation", *Sens. Actuators, A*,vol. 115, no. 2–3, pp. 523–529, 2004, doi: 10.1016/j.sna.2004.04.026.

[3] P.D. Mitcheson, E.M. Yeatman, G.K. Rao, A.S. Holmes, and T.C. Green, "Energy harvesting from human and machine motion for wireless electronic devices", *Proc. IEEE*, vol. 96, no. 9, pp. 1457–1486, 2008, doi: 10.1109/ JPROC.2008.927494.

[4] M. Ostrowski, B. Błachowski, M. Bocheński, D. Piernikarski, P. Filipek, and W. Janicki, "Design of nonlinear electromagnetic energy harvester equipped with mechanical amplifier and spring bumpers", *Bull. Pol. Acad. Sci. Tech. Sci.* vol. 68, no. 6, pp. 1373–1383, 2020, doi: 10.24425/bpasts.2020.135384.

[5] A. Anand, S. Pal, and S. Kundu, "Multi-perforated Energy-Efficient Piezoelectric Energy Harvester Using Improved Stress Distribution", *IETE J. Res.*, pp. 1–16, 2021, doi: 10.1080/ 03772063.2021.1913071.

[6] A. Anand, S. Naval, P.K. Sinha, N.K. Das, and S. Kundu, "Effects of coupling in piezoelectric multi-beam structure", *Microsyst. Technol.*, vol. 26, no. 4, pp. 1235–1252, 2020, doi: 10.1007/s00542-019-04653-3.

[7] A. Anand, and S. Kundu, "Improvement of Output Power in Piezoelectric Energy Harvester under Magnetic Influence", *Proceedings of 3rd International Conference on 2019 Devices for Integrated Circuit (DevIC 2019 IEEE)*, 2019, pp. 382–385, doi: 10.1109/DEVIC.2019.8783607.

[8] A. Anand and S. Kundu, "Design of a spiral-shaped piezoelectric energy harvester for powering pacemakers", *Nanomater. Energy*, vol. 8, no. 2, pp. 139–150, 2019, doi: 10.1680/jnaen.19.00016.

[9] A. Anand and S. Kundu, "Design of Mems Based Piezoelectric Energy Harvester for Pacemaker", *Proceedings of 3rd International Conference on Devices for Integrated Circuit (DevIC 2019)*, 2019, pp. 465–469, doi: 10.1109/DEVIC.2019.8783311.

[10] S. Roundy, P.K. Wright, and J. Rabaey, "A study of low level vibrations as a power source for wireless sensor nodes", *Comput. Commun.*, vol. 26, no. 11, pp. 1131–1144, 2003, doi: 10.1016/S0140-3664(02)00248-7.

[11] S. Naval, P.K. Sinha, N.K. Das, A. Anand, and S. Kundu, "Wideband piezoelectric energy harvester design using parallel connection of multiple beams", *Int. J. Nanopart.*, vol. 12, no. 3, pp. 206–223, 2020, doi: 10.1504/IJNP.2020. 109545.

[12] S. Naval, P.K. Sinha, N.K. Das, A. Anand, and S. Kundu, "Bandwidth Increment of Piezoelectric Energy Harvester using Multibeam Structure", *Proceedings of 3rd International Conference on 2019 Devices for Integrated Circuit (DevIC 2019)*, 2019, pp. 370–373, doi: 10.1109/DEVIC.2019.8783724.

[13] H. S. Kim, J. H. Kim, and J. Kim, "A review of piezoelectric energy harvesting based on vibration", *Int. J. Precis. Eng. Manuf.*, vol. 12, no. 6, pp. 1129–1141, 2011, doi: 10.1007/s12541-011-0151-3.

[14] K. Sokół,"Passive control of instability regions by means of piezoceramic elements", *Lat. Am. J. Solids Struct.*, vol. 18, no. 1, p. e320, 2021, doi: 10.1590/1679-7825 6015.

[15] H. Irschik, "A review on static and dynamic shape control of structures by piezoelectric actuation", *Eng. Struct.*, vol. 24, no. 1, pp. 5–11, 2002, doi: 10.1016/S0141-0296(01)00081-5.

[16] J. Peng, G. Zhang, M. Xiang, H. Sun, X. Wang, and X. Xie, "Vibration control for the nonlinear resonant response of a piezoelectric elastic beam via time-delayed feedback", *Smart Mater. Struct.*, vol. 28, no. 9, p. 095010, 2019, doi: 0000-0003-0104-522X.

[17] H. Hu, Y. Han, A. Song, S. Chen, C. Wang, and Z. Wang, "A finger-shaped tactile sensor for fabric surfaces evaluation by 2-dimensional active sliding touch", *Sensors,* vol. 14, no. 3, pp. 4899–4913, 2014, doi: 10.3390/ s140304899.

[18] M. F. Daqaq, R. Masana, A. Erturk, and D. Dane Quinn, "On the role of nonlinearities in vibratory energy harvesting: a critical review and discussion", *Appl. Mech. Rev.*, vol. 66, no. 4, p. 040801, 2014, doi: 10.1115/1.4026278.

[19] V.R. Challa, M.G. Prasad, Y. Shi, and F.T. Fisher, "A vibration energy harvesting device with bidirectional resonance frequency tunability", *Smart Mater. Struct.*, vol. 17, no. 1, p. 015035, 2008, doi: 10.1088/0964-1726/17/01/ 015035.

[20] D.A. Barton, S.G. Burrow, and L.R. Clare, "Energy harvesting from vibrations with a nonlinear oscillator", *J. Vib. Acoust.,* vol. 132, no. 02, 2010, doi: 10.1115/1.4000809.

[21] S.C. Stanton, C.C. McGehee, and B.P. Mann, "Reversible hysteresis for broadband magnetopiezoelastic energy harvesting", *Appl. Phys. Lett.*, vol. 95, no. 17, p. 174103, 2009, doi: 10.1063/1.3253710.

[22] A. Erturk and D.J. Inman, "Broadband piezoelectric power generation on high-energy orbits of the bistable Duffing oscillator with electromechanical coupling", *J. Sound. Vib.,* vol. 330, no. 10, pp. 2339–2353, 2011, doi: 10.1016/j.jsv.2010.11.018.

[23] S. Zhou, J. Cao, A. Erturk, and J. Lin, "Enhanced broadband piezoelectric energy harvesting using rotatable magnets", *Appl. Phys. Lett.*, vol. 102, no. 17, p. 173901, 2013, doi: 10.1063/1.4803445.

[24] S. Zhou, J. Cao, W. Wang, S. Liu, and J. Lin, "Modeling and experimental verification of doubly nonlinear magnet-coupled piezoelectric energy harvesting from ambient vibration", *Smart Mater. Struct.*, vol. 24, no. 5, p. 055008, 2015, doi: 10.1088/0964-1726/24/5/055008.

[25] S. Zhou, J. Cao, D.J. Inman, J. Lin, S. Liu, and Z. Wang, "Broadband tristable energy harvester: modeling and experiment verification", *Appl. Energy*; vol. 133, pp. 33–39, 2014, doi: 10.1016/j.apenergy.2014.07.077.

[26] L. Haitao, Q. Weiyang, L. Chunbo, D. Wangzheng, and Z. Zhiyong, "Dynamics and coherence resonance of tri- stable energy harvesting system", *Smart Mater. Struct.*, vol. 25, no. 1, p. 015001, 2015, doi: 10.1088/0964-1726/ 25/1/015001.

[27] J.Y. Cao, S.X. Zhou, W. Wang, and J. Lin, "Influence of potential well depth on nonlinear tristable energy harvesting", *Appl. Phys. Lett.*, vol. 106, no. 7, p. 173903, 2015, doi: 10.1063/1.4919532.

[28] P. Kim and J. Seok, "A multi-stable energy harvester: dynamic modeling and bifurcation analysis", *J. Sound Vib.*, vol. 333, no. 21, pp. 5525–5547, 2014, doi: 10.1016/j.jsv. 2014.05.054.

[29] Z. Zhou, W. Qin, Y. Yang, and P. Zhu, "Improving efficiency of energy harvesting by a novel penta-stable configuration", *Sens. Actuators, A,*, vol. 265, pp. 297–305, 2017, doi: 10.1016/j.sna.2017.08.039.

[30] D. Tan, Y.G. Leng, and Y.J. Gao, "Magnetic force of piezoelectric cantilever energy harvesters with external magnetic field", *Eur. Phys. J. Spec. Top.*, vol. 224, no. 14, pp. 2839–2853, 2015, doi: 10.1140/epjst/e2015-02592-6.

[31] D. Zhu, S. Roberts, M.J. Tudor, and S.P. Beeby, "Design and experimental characterization of a tunable vibration-based electromagnetic micro-generator", *Sens. Actuators, A,*, vol. 158, no. 2, pp. 284–293, 2010, doi: 10.1016/j.sna.2010.01.002.

[32] W.J. Su, J. Zu, and Y. Zhu, "Design and development of a broadband magnet-induced dual-cantilever piezoelectric energy harvester", *J. Intell. Mater. Syst. Struct.*, vol. 25, no. 4, pp. 430–442, 2014, doi: 10.1177/1045389X 13498315.

[33] D. Guo, X.F. Zhang, H.Y. Li, and H. Li, "Piezoelectric Energy Harvester Array with Magnetic Tip Mass", in *ASME International Mechanical Engineering Congress and Exposition*, 2015, vol. 57403, p. V04BT04A045, doi: 10.1115/IMECE2015-51044.

[34] S.S. Rao, *Vibration of continuous systems*, John Wiley and Sons, Ltd, 2019, doi: 10.1002/9781119424284.